RSC Advances

PAPER

View Article Online
View Journal | View Issue

Cite this: *RSC Adv.*, 2024, **14**, 35638

A dual-response fluorescence sensor for SO_2 derivatives and polarity and its application in real water and food samples†

Jianfeng Wang,‡[a] Ruiji Li,‡[b] Tao Ou,[b] Yamin Fu,[c] Chang Gao[a] and Yehao Yan*[a]

As an important gaseous pollutant, SO_2 derivatives generally exist and significantly threaten the environment and organism health. Meanwhile, polarity is a disease-related indicator in the organism's microenvironment, where an unregulated variation may disturb the physiological metabolisms. Hence, a superior FRET-based fluorescent sensor (TLA) is presented to track polarity and sulfur dioxide derivatives by dual emission channel, *i.e.* an elevated red emission at 633 nm with decreasing polarity as well as a reduced red emission at 633 nm and improved blue emission at 449 nm with increasing concentration of SO_2 derivatives. The probe TLA could sensitively detect SO_2 derivatives with ultra-large Stokes shift (273 nm), excellent stability, high selectivity, and low detection limit. Importantly, TLA can accurately detect sulfur dioxide derivatives in real food as well as water samples. Besides, TLA was also fabricated as testing strips and applied to detect SO_2 derivatives in the solution.

Received 2nd July 2024
Accepted 25th October 2024

DOI: 10.1039/d4ra04805a

rsc.li/rsc-advances

1 Introduction

Sulfur dioxide (SO_2) derivatives are widely recognized as hazardous substances in the environment and organisms.[1–3] Their excessive emission into the atmosphere contributes to the formation of acid rain, posing a significant threat to ecosystems.[4,5] SO_2 derivatives are often used as food additives for sterilization, bleaching and antioxidants.[6,7] The processing of smoked foods also leaves large amounts of SO_2 derivatives in the products. When SO_2 is dissolved in water or inhaled into the body, it hydrates to form sulfite (HSO_3^-/SO_3^{2-}).[8–10] Prolonged exposure to HSO_3^-/SO_3^{2-} can result in severe respiratory, cardiovascular, and neurological diseases.[11,12] Furthermore, the level of polarity usually represents a vital microenvironmental factor in living biological systems.[13,14] It not only reflects the permeability of individual biological membranes but also plays a pivotal role in plenty of metabolic processes such as signaling and metabolism.[15,16] Notably, abnormal alterations in polarity are firmly associated with the emergence of afflictions such as type 2 diabetes mellitus, polycystic kidney disease, cirrhosis of the liver, and Alzheimer's disease.[17–20] Hence, it is of great significance to explore an effective method to detect HSO_3^-/SO_3^{2-} contents and polarity levels.

With the burgeoning progress of detection technologies, various approaches are being applied to monitor HSO_3^-/SO_3^{2-} concentrations such as chromatography, spectrophotometry, and electrochemistry.[21,22] Compared with the above methods, organic molecular fluorescence sensors not only have outstanding sensitivity, selectivity and resolution but also have the characteristics of real-time non-invasive detection of substances, which has attracted more and more attention.[23–25] Generally, the design mechanisms of organic molecular sensors mainly involve intramolecular charge transfer (ICT),[26,27] excited state intramolecular proton transfer (ESIPT),[28,29] and photo-induced electron transfer (PET),[30,31] through bond energy transfer (TBET)[32,33] and Förster resonance energy transfer (FRET).[34,35] Compared with other platforms, FRET-based organic molecular sensors usually exhibit various advantages such as facile design and synthesis, large stokes shift, colorimetric detection and easy post-functionalization.[36,37] Ratiometric fluorescence detection can effectively relieve systematic error from instruments and surroundings by plotting the ratio value of two fluorescence signals, which may promote the accuracy and reproducibility of analysis.[38,39] Although many organic molecular sensors for HSO_3^-/SO_3^{2-} were prepared, only rare sensors that can synchronously detect HSO_3^-/SO_3^{2-} and polarity are available. The previously developed sensors for SO_2 derivatives and polarity were commonly designed based on an intramolecular charge transfer (ICT) transfer platform and generally showed a small Stokes shift.[40,41] Dual-responding sensors generally possess various strengths including

[a]School of Public Health, Jining Medical University, Jining, Shandong, 272067, P. R. China. E-mail: yanyehao_322@163.com

[b]School of Pharmacy, Jining Medical University, Shandong, 276826, P. R. China

[c]School of Chemistry and Chemical Engineering, Hainan University, Haikou 570228, P. R. China

† Electronic supplementary information (ESI) available. See DOI: https://doi.org/10.1039/d4ra04805a

‡ Equal contribution.

a simplified test process, minimal sample consumption and substance interference.[42,43]

Herein, an organic molecular sensor (named TLA) was designed for HSO_3^-/SO_3^{2-} and polarity based on the FRET mechanism with a unique and novel energy donor known as *N*,*N*-dimethyl-4-(1-methyl-1*H*-phenanthro[9,10-*d*]imidazol-2-yl) benzamide. Under the excitation of the donor, TLA emits a deep red emission window at 633 nm, resulting in a larger stokes shift than various types of SO_2 derivative sensors (Table S1†). As a reactive nucleophilic reactor, HSO_3^-/SO_3^{2-} reacts with the vinyl C=C bond in the acceptor moiety by Michael's addition reaction, and the intramolecular FRET process is disrupted. Thereby, the radiometric detection was realized by plotting the function between the ratio of fluorescence intensity (I_{449}/I_{633}) and the additional amounts of HSO_3^-/SO_3^{2-}. Meanwhile, TLA also responds to the variation of polarity levels due to the TICT process in the acceptor fraction, providing a promising approach for the detection of polarity. Innovatively, sensor TLA with large Stokes shift and emission peak distance was developed for HSO_3^-/SO_3^{2} and polarity based on the FRET system. Importantly, TLA was triumphantly applied to detect the contents of HSO_3^-/SO_3^{2-} with high accuracy and reproducibility in actual water and food specimens.

2 Experimental

2.1 Reagents and apparatus

All reagents in this study were purchased from commercial suppliers and directly used according to instructions. Freshly prepared deionized water was used in this experiment. The silica gel for column chromatography used in the experiment had a mesh size of 200–300. All the absorption spectra in the UV-vis range were tested with a spectrophotometer (TU-1901). Fluorescent emission spectra were obtained using the Hitachi F-2700 spectrophotometer with the excitation of 360 nm light (slits: 5.0/5.0 nm, speed: 300 nm min^{-1}, voltage: 700 V).

2.2 Spectral test

Prior to spectroscopic testing, the sensor was precisely weighed and poured into 10.0 mL of DMSO to prepare the stock solution (1.0×10^{-3} mol L^{-1}). The HSO_3^-/SO_3^{2-} and other species used for the test were derived from the previous studies.[44,45] 50 μL of the sensor stock solution was added to a volumetric flask and filled to 10 mL using the mixed solutions of ethanol and PBS buffer (V/V, 5/5, pH 7.4), then different concentrations of HSO_3^-/SO_3^{2-} or various analytes were appended for spectroscopic testing.

2.3 Synthesis of TLA

4-(1-Methyl-1*H*-phenanthro[9,10-*d*]imidazol-2-yl)benzoic acid (1.0 mmol, 352.1 mg), (*E*)-2-(3-cyano-5,5-dimethyl-4-(4-(piperazin-1-yl)styryl)furan-2(5*H*)-ylidene)malononitrile (1.0 mmol, 371.2 mg), 1-(3-dimethyl-aminopropyl)-3-ethylcarbodiimide hydrochloride (EDC, 1.0 mmol, 191.0 mg) and 4-dimethylaminopyridine (DMAP, 0.2 mmol, 24.3 mg) were mixed into dry dichloromethane, and reacted for 36 h in nitrogen atmosphere

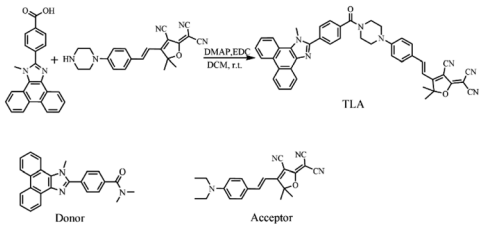

Scheme 1 The preparation route of the probe TLA.

(Scheme 1).[46,47] Then, the products were further purified by using column chromatography with 200–300 mesh silica gel (dichloromethane/methanol, V/V, 50/1). The product TLA was obtained with 26% yield and the structure of TLA was verified by HRMS (ESI): *m*/*z*, $[C_{45}H_{35}N_7O_2D]^+$: 707.2988, found: 707.2980 (Fig. S1†). ^{1}H NMR (500 MHz, DMSO-d_6): 1.77 (s, 6H), 3.61–3.83 (m, 8H), 4.34 (s, 3H), 6.97 (d, J = 16.0 Hz, 1H), 7.04 (d, J = 8.5 Hz, 2H), 7.65–7.83 (m, 8H), 7.65 (d, J = 16.0 Hz, 1H), 7.99 (d, J = 8.0 Hz, 2H) (Fig. S2†). ^{13}C NMR (126 MHz, DMSO-d_6): 26.0, 36.6, 52.5, 55.4, 94.6, 99.1, 110.5, 112.2, 114.5, 121.9, 125.7, 128.1, 136.8, 137.2, 159.2, 151.8, 153.9, 169.2, 176.1, 177.8 (Fig. S3†).

The donor was prepared as Scheme S1,† and determined by ^{1}H NMR (Fig. S4†).

3 Results and discussion

3.1 The design of TLA

Generally, 1-methyl-2-phenyl-1*H*-phenanthro[9,10-*d*]imidazole derivatives possess prominent fluorescence properties, high stability and post-functionalized ability.[48,49] Meanwhile, malononitrile dyes usually exhibit deep red emission windows, excellent photostability and biocompatibility.[50,51] Importantly, the fluorescence emission band well overlaps with the UV-vis absorption band (Fig. S5†), which is beneficial to the energy transfer in FRET and provides a high energy transfer efficiency of 98.02% (Fig. S6†). The optimized molecular structure of TLA was obtained by the Gaussian program, and the result is shown in Fig. S7.† The donor moiety was located on a plane, while the acceptor moiety was located on another plane. The energy gap was calculated to be 2.48 eV. The nucleophilic addition reaction of HSO_3^-/SO_3^{2-} toward the acceptor moiety easily occurred, and caused the destruction of the intramolecular FRET mechanism. Consequently, the signal of the probe was enhanced at 449 nm and weakened at 633 nm, thus achieving the radiometric detection of HSO_3^-/SO_3^{2-} (Scheme 2). Besides, the twisted intramolecular charge transfer would be gradually relieved due

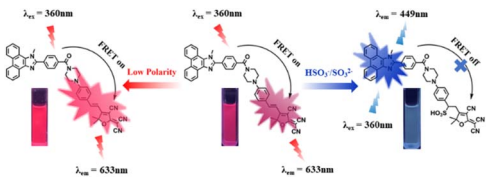

Scheme 2 The responding mechanism of TLA to polarity and HSO_3^-/SO_3^{2}.

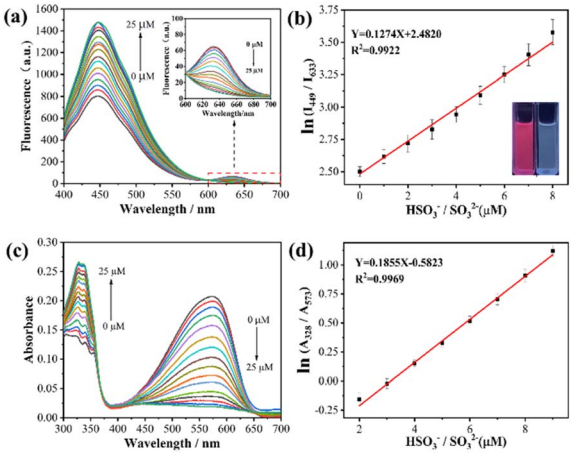

Fig. 1 (a) The fluorescent emission of TLA (5 μM) responding to different contents of HSO_3^-/SO_3^{2-} (0–25 μM). (b) The linearity of $\ln(I_{449}/I_{633})$ to HSO_3^-/SO_3^{2-} concentration (0–8 μM). (c) The absorption spectra of TLA (5 μM) toward the increasing concentrations of HSO_3^-/SO_3^{2-} (0–25 μM) in UV-vis range. (d) The linear relationship between the value of $\ln(I_{328}/I_{573})$ and the concentrations of HSO_3^-/SO_3^{2-} (0–9 μM) (the error bars represent the standard deviation of the three sets of data for each sample).

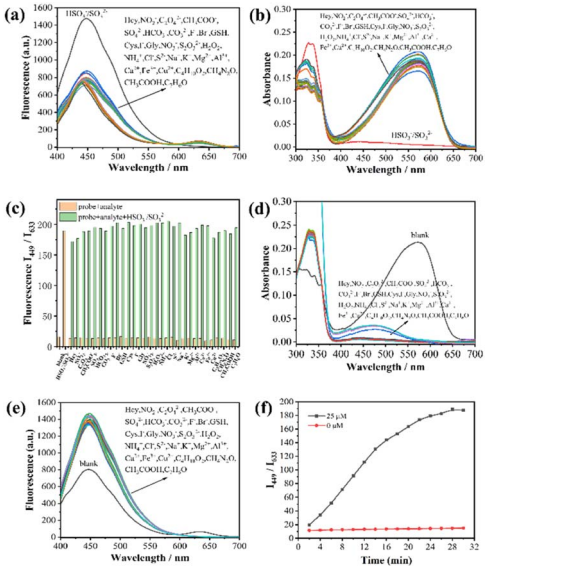

Fig. 2 (a) The fluorescence emission spectra of TLA (5 μM) responding to various analytes. (b) The absorption spectra of TLA (5 μM) responding to various analytes. (c) The I_{449}/I_{633} value of TLA (5 μM) toward HSO_3^-/SO_3^{2-} in the presence of other analytes. (d) The absorption spectra of TLA (5 μM) toward HSO_3^-/SO_3^{2-} in the presence of other analytes. (e) The fluorescence emission spectra of TLA (5 μM) toward HSO_3^-/SO_3^{2-} in the presence of other analytes. (f) The responding time of TLA (5 μM) toward HSO_3^-/SO_3^{2-} (25 μM).

to the decreasing polarity.[52,53] Hence, a dual-response fluorescent sensor for HSO_3^-/SO_3^{2-} and polarity was fabricated.

3.2 Spectral properties of TLA toward HSO_3^-/SO_3^{2-}

To validate the response capacity of TLA for HSO_3^-/SO_3^{2-}, the fluorescence emission spectra of TLA depending on the increasing HSO_3^-/SO_3^{2-} concentration were determined, and the measured results are presented in Fig. 1(a). TLA possessed dual fluorescent emission windows with the enhancing channel at 449 nm and the fading channel at 633 nm with increasing HSO_3^-/SO_3^{2-} concentration. The variation was ascribed to the interruption of the FRET process deriving from the destruction of p-conjugation in the acceptor unit due to the addition reaction of HSO_3^-/SO_3^{2-} toward electron-deficient C=C.[54,55] A good linearity ($R^2 = 0.9922$, $K = 0.1274$) was seen between the $\ln(I_{449}/I_{633})$ value and the HSO_3^-/SO_3^{2-} contents within 0 to 8 μM, which established a premise for the quantitative detection of HSO_3^-/SO_3^{2-} (Fig. 1(b)). Then, the detection limit was calculated as 0.44 μM depending on the formula of LOD = $3\sigma/k$.[56,57] Meanwhile, the UV-vis absorption spectra of TLA toward the increasing HSO_3^-/SO_3^{2-} concentration were further tested and presented in Fig. 1(c). Probe TLA with dual absorption windows and changed oppositely in which the signal was lowered at 573 nm while the signal at 328 nm was heightened upon the addition of HSO_3^-/SO_3^{2-}. The variation originated from the reaction between TLA and HSO_3^-/SO_3^{2-}, which was completely consistent with the result in emission spectra. The $\ln(A_{328}/A_{573})$ was well linearized with the HSO_3^-/SO_3^{2-} concentration with $R^2 = 0.9969$. The above results indicated TLA could quantitatively track the varying HSO_3^-/SO_3^{2-} levels with high accuracy.

The specific recognition was the foremost criterion for the quantitative analysis in complicated environments. To validate the detection selectivity and anti-inference capacity of TLA for HSO_3/SO_3^{2-}, the TLA selectivity toward HSO_3/SO_3^{2-} was explored by letting it react with a variety of analytes. The fluorescence and absorption spectra both indicated that TLA hardly reacts with any analytes (Hcy, NO_2^-, $C_2O_4^{2-}$, CH_3COO^-, SO_4^{2-}, HCO_3^-, CO_3^{2-}, F^-, Br^-, GSH, Cys, I^-, Gly, NO_3^-, $S_2O_3^{2-}$, H_2O_2, NH_4^+, Cl^-, S^{2-}, Na^+, K^+, Mg^{2+}, Al^{3+}, Ca^{2+}, Fe^{3+}, Cu^{2+}, $C_4H_{10}O_2$, CH_4N_2O, CH_3COOH, and C_7H_6O) other than HSO_3^-/SO_3^{2-} (Fig. 2(a) and (b)). Compared with the blank group, the HSO_3^-/SO_3^{2-} existed group changed significantly and the I_{449}/I_{633} value increased 8 times than before (Fig. 2(c)). Subsequently, the same amount of HSO_3^-/SO_3^{2-} was appended to the above testing solutions to analyze their immunity to interference. Both, fluorescence and absorbance spectra indicated that TLA responds well to HSO_3^-/SO_3^{2-} in the presence of other species (Fig. 2(d) and (e)). Consequently, TLA showed the capacity of specific recognition for HSO_3^-/SO_3^{2-} and resistance to interference under complicated conditions.

To reveal the rapid detection feature of TLA for HSO_3^-/SO_3^{2-}, the time-relying kinetic experiments of TLA toward HSO_3^-/SO_3^{2-} were also conducted to confirm the real-time detection. It can be observed that the ratio (I_{449}/I_{633}) of TLA increased gradually and reached a plateau after HSO_3^-/SO_3^{2-} reacted for 30 minutes (Fig. 2(f)), which demonstrated that the sensor was able to detect HSO_3^-/SO_3^{2-} rapidly. Meanwhile, the ratio of I_{449}/I_{633} remained stable in the testing solution revealing the high photostability of TLA. pH-effect was a significant factor for the detection, the response of TLA to HSO_3^-/SO_3^{2-} was investigated under different pH conditions. The values of I_{449}/I_{633} exhibited minimal changes across a pH range of 4–9, indicating a prominent pH-stability of TLA (Fig. S8†). It

can be observed that TLA responded well with HSO_3^-/SO_3^{2-} within the range of pH 6–9, which was more near to the natural, food and organism pH conditions. These results suggested that TLA is better suited for detecting HSO_3^-/SO_3^{2-} under various conditions contributed a wide range of applications.

3.3 Spectral properties of TLA toward polarity

To confirm the polarity-sensitive feature of TLA, the fluorescent spectra of TLA were initially measured in different polar organic solvents involving tetrahydrofuran, dichloromethane, ethanol, *N*,*N*-dimethylformamide and dimethyl sulfoxide. In Fig. 3(a), the emission peak of TLA redshifted from 612 to 642 nm with the increasing solvent polarity. Besides, the polarity titration of TLA was investigated in a mixed solution of PBS and 1,4-dioxane where the polarity was decreased by promoting the solvent content of 1,4-dioxane.[58,59] The fluorescence emission of TLA was raised and blue-shifted gradually with the rising contents of 1,4-dioxane in the test solution, which was attributed to the continuous decrease of polarity (Fig. 3(b)). Meanwhile, an excellent linear relationship between $\ln(I_{633})$ and the 1,4-dioxane proportions in the mixed solvents of 1,4-dioxane and PBS was plotted to be $Y = 0.2163X + 3.8754$ with $R^2 = 0.9838$ in the range of 20–90% (Fig. 3(c)). Moreover, the absorption peak at 540 nm increased clearly while the window at 370 nm weakened obviously with the appending of DCM (Fig. 3(d)). It is clear from the above that TLA can be recognized as a polarity-sensitive sensor by its fluorescence property of increasing with decreasing polarity.

3.4 The recognition mechanism of TLA for HSO_3^-/SO_3^{2-}

To clear the detection essence of TLA, the recognition mechanism of the probe TLA for HSO_3^-/SO_3^{2-} was verified through HRMS and ^1H NMR. The HRMS analysis displayed that *m*/*z* 788.2662 was consistent with the calculation of $[C_{45}H_{38}N_7O_5S]^+$ 788.2650 (Fig. S9†). Besides, in the ^1H NMR spectrum, the dual diagnostic hydrogens (δ = 6.98, 1H and δ = 7.92, 1H) of the olefin disappeared and two hydrogens (δ = 4.93, 1H and δ = 5.07, 1H) were generated with the addition of HSO_3^-/SO_3^{2-} (Fig. S10†). The above evidence indicated the nucleophilic addition reaction of HSO_3^-/SO_3^{2-} toward the olefin group of in probe TLA.

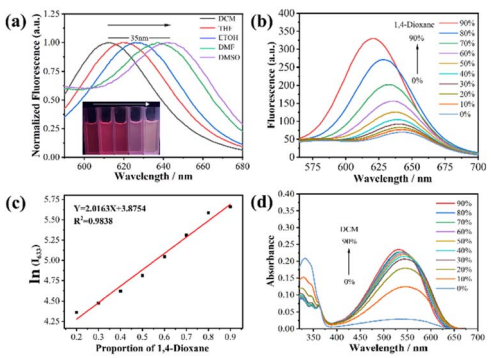

Fig. 3 (a) The fluorescence spectra of TLA in DCM, THF, EtOH, DMF and DMSO. (b) The fluorescence of TLA relying on the decreasing of 1,4-dioxane proportions. (c) The linear relationship of $\ln(I_{633})$ to the increasing proportions of 1,4-dioxane in the mixed solvents of 1,4-dioxane and PBS. (d) The absorbance of TLA for the decreasing of DCM proportions in DCM and DMF mixed solvents.

3.5 Application of TLA in real samples

The outstanding performances in spectral testing encouraging TLA applied to sense HSO_3^-/SO_3^{2-} for real samples. Firstly, the different contents of HSO_3^-/SO_3^{2-} in various real water samples was monitored by TLA, including tap water, yellow river, Daming Lake, Baotu Spring, Taibai Lake and Beijing–Hangzhou canal (Table 1). The spiked recoveries for the above real water samples were distributed at 91.77–118.92%. Moreover, TLA was also employed to measure the HSO_3^-/SO_3^{2-} contents of real food samples involving granulated sugar, beancurd sticks and mushroom. The HSO_3^-/SO_3^{2-} contents in the primeval water samples was not detected, and the values of I_{449}/I_{633} increased significantly depending on the addition of HSO_3^-/SO_3^{2-} (2, 5

Table 1 The contents of HSO_3^-/SO_3^{2-} in real water and food samples

Sample	HSO_3^-/SO_3^{2-} spiked (μM)	HSO_3^-/SO_3^{2-} recovered (μM)	Recovery (%)
Tap water	0	Not detected	—
	2	2.14 ± 0.20	107.32
	5	4.80 ± 0.49	96.19
	8	9.41 ± 0.56	117.63
Yellow River	0	Not detected	—
	2	2.19 ± 0.22	109.79
	5	5.94 ± 0.22	118.92
	8	8.81 ± 0.66	110.14
Daming Lake	0	Not detected	—
	2	2.16 ± 0.16	108.46
	5	4.89 ± 0.09	97.97
	8	7.95 ± 0.37	99.48
Baotu Spring	0	Not detected	—
	2	2.32 ± 0.28	116.49
	5	5.62 ± 0.13	112.52
	8	8.62 ± 0.13	107.85
Taibai Lake	0	Not detected	—
	2	2.22 ± 0.15	111.36
	5	4.88 ± 0.26	97.72
	8	8.55 ± 0.55	106.99
Beijing–Hangzhou canal	0	Not detected	—
	2	1.83 ± 0.15	91.77
	5	5.94 ± 0.53	118.85
	8	7.53 ± 0.57	94.21
Granulated sugar	0	5.03 ± 0.05	—
	2	7.19 ± 0.18	108.01
	5	10.80 ± 0.11	115.45
	8	14.05 ± 0.31	112.76
Grape wine	0	9.45 ± 0.33	—
	2	11.25 ± 0.19	90.27
	5	14.53 ± 0.43	101.65
	8	17.18 ± 0.05	96.65
Mushroom	0	5.90 ± 0.04	—
	2	8.16 ± 0.01	112.98
	5	10.42 ± 0.13	90.44
	8	13.53 ± 0.40	95.32
Dried beancurd sticks	0	8.78 ± 0.01	—
	2	11.08 ± 0.07	114.88
	5	13.65 ± 0.06	97.33
	8	16.54 ± 0.15	96.96

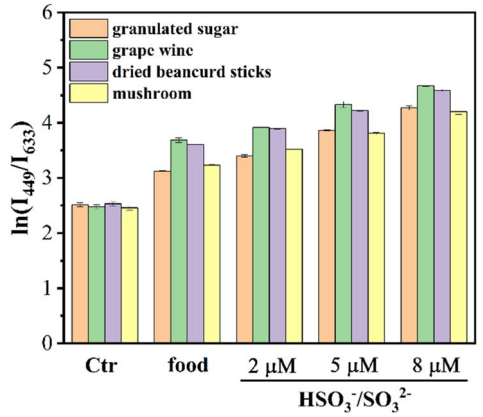

Fig. 4 The fluorescence ratio $\ln(I_{449}/I_{633})$ of TLA to HSO_3^-/SO_3^{2-} in real food samples (the error bars represent the standard deviation of the three sets of data for each sample).

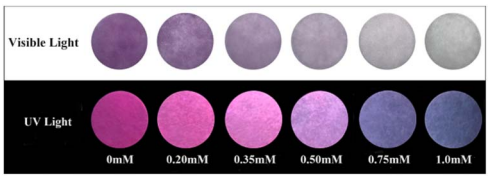

Fig. 5 The color variation of TLA (0.2 mM) soaked test strips toward different concentrations of Na_2SO_3 including 0, 0.20, 0.35, 0.50, 0.75 and 1.0 mM (under visible light and 365 nm UV light).

and 8 μM) in real food samples (Fig. 4). The HSO_3^-/SO_3^{2-} contents were also respectively obtained to be 0.03, 0.11 and 0.07 g kg^{-1}, and for grape wine was calculated to be 0.12 g L^{-1}.[60–63] Meanwhile, the spiked recoveries of exogenous HSO_3^-/SO_3^{2-} in real food samples were mainly distributed in 90.44–115.45%. The above-tested data effectively illustrates that the TLA probe was suitable to sense HSO_3^-/SO_3^{2-} contents for real water and food samples.

Test strips were used in a wide range of applications as a convenient and fast test tool with visualization capabilities. In view of the results of the above optical tests on the probe TLA, we found that the color was slowly converted from a dark purple to a lighter color with the addition of HSO_3^-/SO_3^{2-}. Therefore, we prepared the probe TLA as a sodium–sulfur test strip for the visual detection of aqueous sulfur dioxide solutions. As shown in Fig. 5, the test paper is dark purple when sodium sulfite is not present and it gradually becomes colorless as the amount of sodium sulfite increases. Under the irradiation of ultraviolet light, the test paper changes from purplish red to light blue. This means that the probe TLA has the potential to be made into test trips that can be used to visually detect sodium sulfite in the environment.

4 Conclusions

This work involved the design and synthesis of a FRET-based fluorescence sensor TLA for dual-response of sulfite and polarity. TLA with a novel energy donor exhibited excellent properties in the sensing of sulfite including large Stokes shift, wide fluorescence peak gap, low detection limit, outstanding sensitivity and selectivity. Besides, TLA could also sense polarity degree with an excellent linear relationship over a wide range of polarity. Significantly, TLA was successfully employed to sense the contents of HSO_3^-/SO_3^{2-} in real water and food samples with high accuracy, reproducibility and sensitivity. The testing strips of TLA have also been produced to visualize the HSO_3^-/SO_3^{2-} levels with the naked eye.

Data availability

Details of ESI† are available at **https://doi.org/10.1039/d4ra04805a**.

Author contributions

Jianfeng Wang: data curation, investigation, validation. Ruiji Li: methodology, validation. Tao Ou: investigation. Yamin Fu: methodology. Chang Gao: investigation, supervision. Yehao Yan: resources, funding acquisition, supervision, writing – original draft, writing-review and editing.

Conflicts of interest

There are no conflicts to declare.

Acknowledgements

This work was supported by the Natural Science Foundation of Shandong Province (ZR2021QB184) and the National Natural Science Foundation of China (22304039).

References

1 H. Peng, S. Kong, X. Deng, Q. Deng, F. Qi, C. Liu and R. Tang, *J. Agric. Food Chem.*, 2023, **71**, 14322–14329.
2 C. Bian, S. Zhang, J. Fan, S. Chen, M. Yu and Z. Li, *Dyes Pigm.*, 2023, **216**, 111308.
3 F. T. Liu, N. Li, Y. S. Chen, H. Y. Yu, J. Y. Miao and B. X. Zhao, *Anal. Chim. Acta*, 2022, **1211**, 339908.
4 Z. Ye, C. Duan, R. Sheng, J. Xu, H. Wang and L. Zeng, *Talanta*, 2018, **176**, 389–396.
5 S. Sun, K. Xue, Y. Zhao and Z. Qi, *Talanta*, 2024, **270**, 125568.
6 F. Li, S. M. Zhai, J. J. Xian-Yu, B. X. Zhao and Z. M. Lin, *Talanta*, 2024, **271**, 125684.
7 S. Xu, R. Tang, Z. Wang, Y. Zhou and R. Yan, *Spectrochim. Acta, Part A*, 2015, **149**, 208–215.
8 Y. Li, X. Sun, L. Zhou, L. Tian, K. Zhong, J. Zhang, X. Yan and L. Tang, *J. Agric. Food Chem.*, 2022, **70**, 10899–10906.
9 F. Li, B. Z. Zhou, W. Yao, S. K. Sun, J. Y. Miao, B. X. Zhao and Z. M. Lin, *Anal. Chim. Acta*, 2023, **1239**, 340721.
10 X. Song, Y. Guo, C. Jing, Y. Feng, C. Cao, M. Kou, W. Liu and D. Wang, *Anal. Chem.*, 2022, **94**, 5744–5751.
11 J. Xu, J. Pan, X. Jiang, C. Qin, L. Zeng, H. Zhang and J. F. Zhang, *Biosens. Bioelectron.*, 2016, **77**, 725–732.

12 F. T. Liu, P. F. Jiang, Y. P. Wang, B. X. Zhao and Z. M. Lin, *Anal. Chim. Acta*, 2024, **1288**, 342184.
13 B. Zheng, Y. Tian, S. Liu, J. Yang, F. Wu and H. Xiong, *Anal. Chem.*, 2023, **95**, 12054–12061.
14 W. Zhu, Q. Li, S. Gong and G. Feng, *Anal. Chim. Acta*, 2023, **1278**, 341748.
15 M. Qian, L. Zhang, Z. Pu, C. Zhang, Q. Chen, X. Sui, X. Han, S. Zeng, H. Cui, J. Wang and X. Peng, *Sens. Actuators, B*, 2021, **344**, 130261.
16 Y. Huang, M. Li, Q. Zan, R. Wang, S. Shuang and C. Dong, *Anal. Chem.*, 2023, **95**, 10155–10162.
17 L. Fan, X. Wang, Q. Zan, L. Fan, F. Li, Y. Yang, C. Zhang, S. Shuang and C. Dong, *Anal. Chem.*, 2021, **93**, 8019–8026.
18 J. Zhang, W. Han, X. Zhou, X. Zhang, H. Zhang, T. Li, J. Wang, Y. Yuan, Y. He and J. Zhou, *Anal. Chem.*, 2023, **95**, 11785–11792.
19 S. Zhang, H. Zheng, L. Yang, Z. Li and M. Yu, *Anal. Chem.*, 2023, **95**, 5377–5383.
20 C. Liu, J. Yin, B. Lu and W. Lin, *Sens. Actuators, B*, 2021, **346**, 130448.
21 Z. Shang, M. Wu, Q. Meng, Y. Jiao, Z. Zhang and R. Zhang, *J. Hazard. Mater.*, 2024, **465**, 133165.
22 S. Zhang, X. Yang, Y. Xu, H. Wang, F. Luo, G. Fu, D. Yan, M. Lai, Y. Ke, Y. Ye and X. Ji, *Food Chem.*, 2024, **439**, 138151.
23 Y. Li, X. Jiang, Y. Li, X. Yan, L. Tang, X. Sun, K. Zhong, X. Li and J. Li, *Food Chem.*, 2024, **458**, 140239.
24 P. Das, S. Ganguly, S. Banerjee and N. C. Das, *Res. Chem. Intermed.*, 2019, **45**, 3823–3853.
25 L. Tang, H. Yu, K. Zhong, X. Gao and J. Li, *RSC Adv.*, 2019, **9**, 23316–23323.
26 X. L. Liu, M. Yan, Z. G. Chen, B. Zhang, N. Yao, S. Zhao, X. Zhao, T. Zhang and G. Hai, *Spectrochim. Acta, Part A*, 2023, **286**, 121955.
27 K. Xu, N. Tang, F. Liu, Y. Ai, H. Ding, C. Fan, G. Liu and S. Pu, *Spectrochim. Acta, Part A*, 2024, **317**, 124415.
28 Y. L. Tang, P. He, K. Zhong, S. Hou and Y. Bian, *Spectrochim. Acta, Part A*, 2016, **169**, 246–251.
29 H. Ren, F. Huo, X. Wu, X. Liu and C. Yin, *Chem. Commun.*, 2021, **57**, 655–658.
30 J. Lan, L. Liu, Z. Li, R. Zeng, L. Chen, Y. He, H. Wei, Y. Ding and T. Zhang, *Talanta*, 2024, **267**, 125104.
31 L. Bu, X. Ma, A. Ji, K. Geng, H. Feng, L. Li, A. Zhang and Z. Cheng, *Eur. J. Nucl. Med. Mol. Imaging*, 2024, **51**, 656–668.
32 W. Hu, L. Zeng, S. Zhai, C. Li, W. Feng, Y. Feng and Z. Liu, *Biomaterials*, 2020, **241**, 119910.
33 S. Su, L. Chai, Q. An, W. Hu, L. Wang, X. Li, H. Zhang and C. Li, *Anal. Chem.*, 2022, **94**, 15146–15154.
34 D. Yang, X. Y. He, X. T. Wu, H. N. Shi, J. Y. Miao, B. X. Zhao and Z. M. Lin, *J. Mater. Chem. B*, 2020, **8**, 5722–5728.
35 B. Y. Wei, C. Y. Zhao, M. M. Xiao, Y. Zheng, F. Li, J. Y. Miao, B. X. Zhao and Z. M. Lin, *Spectrochim. Acta, Part A*, 2024, **305**, 123541.
36 Z. Y. Li, M. M. Xiao, Y. Zheng and B. X. Zhao, *Spectrochim. Acta, Part A*, 2022, **279**, 121397.
37 C. Chen, C. Zhou, W. Yang and Y. Hu, *Spectrochim. Acta, Part A*, 2023, **300**, 122902.
38 F. T. Liu, S. Wang, Y. P. Wang, P. F. Jiang, J. Y. Miao, B. X. Zhao and Z. M. Lin, *Talanta*, 2024, **275**, 126135.
39 Z. Wang, R. Liu, Z. Fu, X. Yi, Y. Hu, C. Liu, D. Pan and Z. Wu, *Anal. Methods*, 2023, **15**, 2505–2511.
40 P. Xie, J. Liu, X. Yang, W. Zhu and Y. Ye, *Sens. Actuators, B*, 2022, **365**, 131937.
41 S. Ma, K. Wang, X. Yu, Y. Zhang, M. Xing, X. Wu, D. Cao and Z. Liu, *Dyes Pigm.*, 2020, **182**, 108691.
42 C. Fang, Q. Deng, K. Zhao, Z. Zhou, X. Zhu, F. Liu, P. Yin, M. Liu, H. Li, Y. Zhang and S. Yao, *Anal. Chem.*, 2024, **96**, 3436–3444.
43 L. Ma, Q. Zan, B. Zhang, W. Zhang, C. Jia and L. Fan, *Anal. Bioanal. Chem.*, 2024, **416**, 1375–1387.
44 W. Ai, Y. Bu, H. Huang, J. Wang, M. Ren, Y. Deng, Y. Zhu, S. Wang, Z. P. Yu and H. Zhou, *Anal. Chem.*, 2023, **95**, 6287–6294.
45 M. J. Hou, Z. Q. Wang, J. T. Chen, Z. K. Tan, G. J. Mao, D. H. Chen, Y. Li and C. Y. Li, *Talanta*, 2023, **265**, 124815.
46 W. Wu, L. Zhao, Y. Zhang, J. Wei, J. Han, Y. Zhang and Z. Zhao, *Sci. Rep.*, 2024, **14**, 1336.
47 H. Zhang, L. L. Li, L. Shi, S. Y. Chen, K. Li and X. Q. Yu, *Chem. Commun.*, 2022, **58**, 13720–13723.
48 G. G. Dias, O. R. M, E. R. S. Paz, P. N. M, M. H. Araujo, F. S. Rodembusch and E. N. da Silva Junior, *ACS Sens.*, 2022, **7**, 2865–2919.
49 C. S. Kwan, T. Wang, S. M. Chan, Z. Cai and K. C. Leung, *Dalton Trans.*, 2020, **49**, 5445–5453.
50 M. Wang, X. Han, X. Yang, J. Liu, X. Song, W. Zhu and Y. Ye, *Analyst*, 2021, **146**, 6490–6495.
51 J. Chen, Z. Peng, M. Ji and P. Wang, *Bioorg. Chem.*, 2023, **138**, 106655.
52 M. Kamaci and I. Kaya, *J. Fluoresc.*, 2015, **25**, 1339–1349.
53 B. Lin, Z. Li, Q. Zan, L. Fan, Y. Shu and J. Wang, *Analyst*, 2023, **148**, 3285–3294.
54 J. Wang, Y. Liu, Z. Shang, C. Dong, Y. Wang and S. Shuang, *Anal. Chim. Acta*, 2023, **1279**, 341786.
55 Y. Ye, C. Liu, L. Wang, X. C. Shen and H. Chen, *Talanta*, 2022, **249**, 123699.
56 Y.-M. Tian, S.-S. Liu, W.-N. Wu, X.-L. Zhao, Y. Wang, Y.-C. Fan, Z.-H. Xu and T. D. James, *Sens. Actuators, B*, 2024, **409**, 135496.
57 P. Das, S. Ganguly, S. Mondal, M. Bose, A. K. Das, S. Banerjee and N. C. Das, *Sens. Actuators, B*, 2018, **266**, 583–593.
58 T. Peng, J. Chen, R. Liu and J. Qu, *Spectrochim. Acta, Part A*, 2024, **314**, 124198.
59 J. Ge, Z. Wang, Y. Deng, F. Ding, J. Wang, X. Shen, C. Zhang, C. Wang, L. Hu and H. Wang, *Spectrochim. Acta, Part A*, 2024, **318**, 124479.
60 F. T. Liu, S. M. Zhai, D. F. Gao, S. H. Yang, B. X. Zhao and Z. M. Lin, *Anal. Chim. Acta*, 2024, **1305**, 342588.
61 D. Zhang, S. Wang, F. Yang, Z. Li and W. Huang, *Food Chem.*, 2023, **408**, 135200.
62 C. Yue, L. Zeng, D. Zhang, K. Li, L. Jiang and P. Xie, *Food Chem.*, 2024, **440**, 138183.
63 W. Lu, W. Wang, S. Zhang and W. Li, *Talanta*, 2022, **243**, 123334.